Anatomy and Dynamics of a Supramolecular Membrane Protein Cluster

Jochen J. Sieber, *et al.*

(6), and the highly divergent Cvi-0 (13). In C24, the S locus is extensively rearranged as compared with that of Col-0, and ΨSCR is deleted (14), whereas in Cvi-0, the S locus is similar in structure to Col-0 but is highly diverged in sequence (Fig. 1A). Most of the sequence between the U-box gene and ΨSRK cannot be aligned for the three haplotypes. Cvi-0 SCR carries no obvious null mutation, whereas Cvi-0 ΨSRK has a distinctive splice-site change (fig. S1).

Because we found high variation, our data rule out the fixation of a single loss-of-function allele at the S locus as a key step in the transition to selfing. Instead, the ancestral balanced polymorphism at the S locus is gradually being eroded through genetic drift, perhaps in combination with selection for inactivity: a process that may be very slow, especially in highly structured populations. The A. thaliana SRK alleles are shared with closely related species (15). Given that linkage disequilibrium (LD) extends throughout the S-locus region (Fig. 1B), it seems likely that the same will be true for SCR. At the same time, the observation that transformation with S-locus alleles from A. lyrata does not always restore self-incompatibility (6) suggests multiple evolutionary routes to selfing.

Our results contradict a report of low variability at ΨSCR (but not ΨSRK) resulting from a recent selective sweep (12). The disagreement is not due to differences in the sample that was used: We were unable to replicate previously published results (12) using the published PCR primers and accessions (table S1 and fig. S2), and the reported ΨSCR sequence in Cvi-0 disagrees with our BAC sequence, although the highly divergent ΨSRK is identical in our BAC sequence and in the sequence in the previous report. We therefore conclude that the published results are erroneous.

It has been noted that a selective sweep at SCR, but not SRK, seemed unlikely (15): Our data resolve this contradiction.

Finally, we considered when selfing might have evolved. It has been estimated that SRK started to become a pseudogene no more than 413,000 years ago (15); however, the transition to selfing could have taken place earlier if loss of S-locus function was not the first step [as suggested by the discovery of a modifier of self-incompatibility in A. thaliana (16)]. To obtain an alternative estimate, we examined the genome-wide pattern of LD (11). LD in a partially selfing organism should decay like that in an outcrosser, albeit more slowly (17). However, a very different pattern is expected with a recent, dramatic change in outcrossing, because recombination events that took place before the transition to selfing would have been more effective in breaking up LD. As a result, long-range LD, which reflects recent events, should be too high relative to short-range LD, which reflects more ancient events. This pattern should be detectable unless selfing evolved either a very long time ago (on the order of the coalescence time, or about 10^6 years in A. thaliana) or very recently, in which case the LD pattern should still look like that of an outcrosser. The LD decay reveals no indication of a recent change in selfing (Fig. 1, C and D), and because the LD pattern is very different from that in an outcrosser, species-wide selfing most likely evolved on the order of a million years ago or more. This would also have provided ample time for the suite of selfing-associated traits that distinguish A. thaliana from A. lyrata to evolve (3).

References and Notes
1. S. C. H. Barrett, *Nat. Rev. Genet.* **3**, 274 (2002).
2. M. Koch, B. Haubold, T. Mitchell-Olds, *Am. J. Bot.* **88**, 534 (2001).
3. D. Charlesworth, X. Vekemans, *Bioessays* **27**, 472 (2005).
4. J. B. Nasrallah, *Curr. Opin. Plant Biol.* **3**, 368 (2000).
5. M. Kusaba et al., *Plant Cell* **13**, 627 (2001).
6. M. E. Nasrallah, P. Liu, S. Sherman-Broyles, N. A. Boggs, J. B. Nasrallah, *Proc. Natl. Acad. Sci. U.S.A.* **101**, 16070 (2004).
7. J. Maynard Smith, J. Haigh, *Genet. Res.* **23**, 23 (1974).
8. N. L. Kaplan et al., *Genetics* **123**, 887 (1989).
9. T. R. Ioerger, A. G. Clark, T.-H. Kao, *Proc. Natl. Acad. Sci. U.S.A.* **87**, 9732 (1990).
10. Materials and methods are available as supporting material on *Science* Online.
11. R. M. Clark et al., *Science* **317**, 338 (2007).
12. K. K. Shimizu et al., *Science* **306**, 2081 (2004).
13. M. Nordborg et al., *PLoS Biol.* **3**, e196 (2005).
14. S. Sherman-Broyles et al., *Plant Cell* **19**, 94 (2007).
15. J. S. Bechsgaard, V. Castric, D. Charlesworth, X. Vekemans, M. H. Schierup, *Mol. Biol. Evol.* **23**, 1741 (2006).
16. P. Liu, S. Sherman-Broyles, M. E. Nasrallah, J. B. Nasrallah, *Curr. Biol.* **17**, 734 (2007).
17. M. Nordborg, *Genetics* **154**, 923 (2000).
18. C. Mayor et al., *Bioinformatics* **16**, 1046 (2000).
19. J. C. Barrett, B. Fry, J. Maller, M. J. Daly, *Bioinformatics* **21**, 263 (2005).
20. This study was funded by NSF grant DEB-0115062 to M.N., NIH Center of Excellence in Genomic Science grant P50 HG002790 to M. Waterman, NSF grant IBN-0414521 to M. E. Nasrallah and J.B.N., NIH grant GM62932 to J. Chory and D.W., and the Max Planck Society. The GenBank accession number for the Cvi-0 BAC sequence is EF637083. We thank M. Koornneef for access to the Cvi-0 BAC library.

Anatomy and Dynamics of a Supramolecular Membrane Protein Cluster

Jochen J. Sieber,[1] Katrin I. Willig,[2] Carsten Kutzner,[3] Claas Gerding-Reimers,[1] Benjamin Harke,[2] Gerald Donnert,[2] Burkhard Rammner,[4] Christian Eggeling,[2] Stefan W. Hell,[2] Helmut Grubmüller,[3] Thorsten Lang[1]†

Most plasmalemmal proteins organize in submicrometer-sized clusters whose architecture and dynamics are still enigmatic. With syntaxin 1 as an example, we applied a combination of far-field optical nanoscopy, biochemistry, fluorescence recovery after photobleaching (FRAP) analysis, and simulations to show that clustering can be explained by self-organization based on simple physical principles. On average, the syntaxin clusters exhibit a diameter of 50 to 60 nanometers and contain 75 densely crowded syntaxins that dynamically exchange with freely diffusing molecules. Self-association depends on weak homophilic protein-protein interactions. Simulations suggest that clustering immobilizes and conformationally constrains the molecules. Moreover, a balance between self-association and crowding-induced steric repulsions is sufficient to explain both the size and dynamics of syntaxin clusters and likely of many oligomerizing membrane proteins that form supramolecular structures.

The fluid mosaic model for the structure of biological membranes (1) proposes that individual membrane proteins diffuse freely in a sea of lipids. However, it is becoming clear that most membrane proteins are organized in clusters that are diverse. Current popular theories for membrane compartmentalization do not provide a satisfactory explanation for this degree of micropatterning. For instance, partitioning selected components into lipid rafts is supposed to organize the membrane (2), but whereas glycosyl-phosphatidyl (GPI)–anchored proteins enrich in rafts, the large majority of transmembrane proteins prefer the nonraft phase. Other models propose subplasmalemmal "fences" and "pickets" to form compartment boundaries (3). However, these theories can explain formation of only a limited number of different plasmalemmal compartments, what is difficult to reconcile with the large compositional diversity of membrane domains. Thus, the physical principles underlying most membrane protein clusters are not yet adequately understood.

Several observations are consistent with highly specific clustering mechanisms. Particularly striking are observations that several integral membrane protein isoforms or structurally similar family members segregate in nonoverlapping clusters, including receptors (4), lipid phosphate phosphatases (5), and members of the soluble N-ethylmaleimide–sensitive factor attachment pro-

tein receptor (SNARE) family [so-called syntaxins (6, 7)]. Segregation of syntaxins is likely functionally important because syntaxin 1 and 4 clusters represent sites for docking and fusion of secretory granules and caveolae, respectively (8–10). In vitro, syntaxin 1 forms homo-oligomers via its SNARE motif (11), and, although most syntaxin clusters are also stabilized by cholesterol [for example, (6, 8–10)], it has been shown that for specific cluster formation homophilic interactions of the SNARE motifs are essential (7). This renders a self-organizing system governed by protein-protein interactions, a plausible biological mechanism, explaining the high specificity of cluster formation. Unfortunately, the existence, let alone the mechanism, of such a self-organizing process could so far not be established because of limited knowledge about the size, composition, and dynamics of the clusters.

To overcome this limitation, we have combined the nanoresolving power of stimulated emission depletion (STED) fluorescence microscopy (fig. S1) (12–14) with quantitative biochemistry, fluorescence recovery after photobleaching (FRAP) analysis, and simulations to determine the physical basis of the supramolecular nanostructure formed by syntaxin 1.

[1]Department of Neurobiology, Max Planck Institute for Biophysical Chemistry, Am Fassberg 11, 37077 Göttingen, Germany. [2]Department of Nanobiophotonics, Max Planck Institute for Biophysical Chemistry, Am Fassberg 11, 37077 Göttingen, Germany. [3]Department of Theoretical and Computational Biophysics, Max Planck Institute for Biophysical Chemistry, Am Fassberg 11, 37077 Göttingen, Germany. [4]Friedensallee 92, 22763 Hamburg, Germany.

†To whom correspondence should be addressed. E-mail: tlang@gwdg.de

In neuroendocrine PC12 cells, the density of syntaxin clusters per surface area plasma membrane was quantified by STED microscopy on membrane sheets (Fig. 1A). STED microscopy reaches resolutions far below that of conventional light microscopy (12–14) and is able to separate individual clusters (Fig. 1A). Featuring a focal plane resolution of 50 nm, that is, ~5 times beyond the diffraction barrier, the STED microscope revealed an average density of 19.6 clusters per μm^2 (Fig. 1A). To estimate the total number of clusters, we further determined the average cell surface area by confocal microscopy (460 μm^2; fig. S2). Accordingly, a cell contains about 9000 clusters. Quantitative immunoblotting revealed an average of 830,000 syntaxin 1 copies per cell (fig. S3), yielding a syntaxin/cluster ratio of 90, which is an upper estimate (15). STED microscopy also revealed an average cluster diameter of 50 to 60 nm (Fig. 1B) (15), suggesting that within the cluster syntaxin molecules are densely packed.

To examine the mobility of syntaxin in the plasma membrane, we performed FRAP experiments in living PC12 cells expressing green fluorescent protein (GFP)–labeled syntaxin 1A. This method determines the overall mobility, although it is not able to differentiate between clustered and freely moving molecules. As shown in Fig. 2, fluorescence recovery times ranged from 40 to 60 s, much higher than expected for a freely diffusing protein with a single transmembrane region (TMR) [(16); for diffusion coefficients, see (15)], and full recovery was not reached in the course of the experiment. To exclude the possibility that incomplete recovery is a bleaching artifact, we performed

FRAP control experiments on membrane sheets that enabled us to correct the signal for bleaching and laser fluctuations because the total fluorescence of the preparation was known. No difference in FRAP was observed between live cells and membrane sheets (fig. S4). This experiment further indicates that cytosolic factors and actin reorganization play no role in controlling syntaxin mobility.

To identify the region of the protein that is responsible for mobility restriction, we studied mutant forms and deletion constructs of syntaxin 1A. Syntaxin 1A contains a C-terminal TMR, a membrane-adjacent SNARE motif, and an independently folded N-terminal domain connected to the SNARE motif via a linker region (17) (Fig. 2B). It has been previously shown that syntaxin can form oligomers via its TMRs (18) and can adopt a closed conformation in which the N-terminal domain is folded back onto the SNARE motif (19). In FRAP experiments, mutations that prevent TMR oligomerization (18) or the closed conformation (19) behaved indistinguishably from wild-type syntaxin (Fig. 2B), indicating that these mechanisms have no strong influence on syntaxin mobility. However, mobility increased dramatically after deleting most of syntaxin's cytoplasmatic part, and restriction in mobility could be rescued by adding back the SNARE motif (Fig. 2C). Shortening the N-terminal part of the SNARE motif gradually increased mobility from region –5 on, with almost maximal mobility observed after deletion of region –3 (Fig. 2, D and F). Thus, the part from –5 to –3 is essential for restricted mobility. However, it is not sufficient, because construct –5Δ (Fig. 2F), containing –5 to –3 but lacking the

A   Density of Sx1 clusters
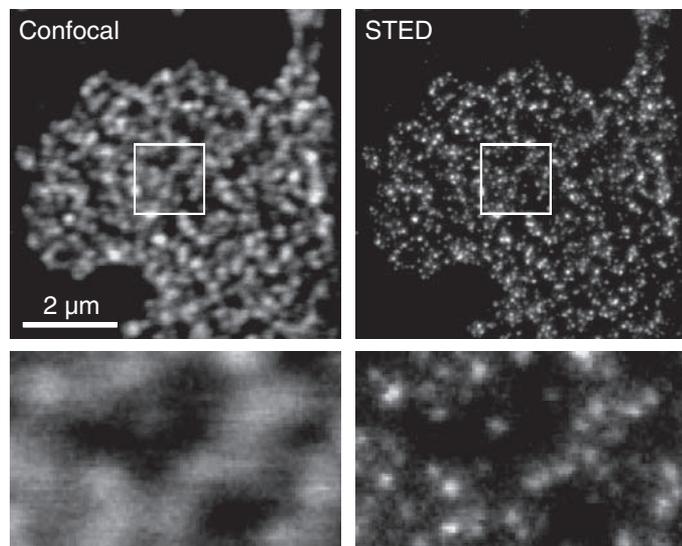
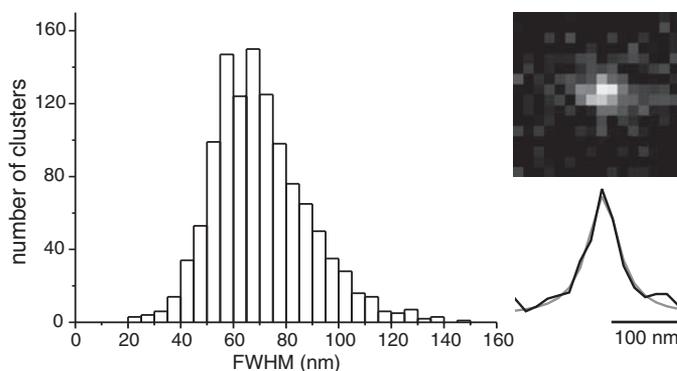## B   Histogram of measured Sx1 cluster size

Fig. 1. Syntaxin 1 clusters in PC12 cells. (**A**) Syntaxin 1 clusters were visualized by antibody staining for which access to the inner leaflet of the plasma membrane is a prerequisite. To avoid detergent permeabilization of the plasma membrane that may lead to artificial protein distribution, we removed the upper parts of the cells by a brief ultrasound treatment (fig. S4) and immunostained the remaining plasma membrane sheets after fixation. In contrast to their confocal counterparts (left), nanoscale-resolution STED micrographs (right) reveal that syntaxin concentrates in clusters at an average density of 19.6 ± 5.7 per μm^2 (mean ± SD, n = 47 membrane sheets). Bottom images are magnified views from boxed regions in top images. (**B**) Histogram showing the distribution of full width at half maximum (FWHM) of syntaxin 1 cluster signals obtained from STED micrographs by line scan analysis (median = 68 nm; 1166 clusters from 25 membrane sheets). The FWHM of individual clusters was determined from the Lorentzian fit (gray line) of the line scan (black line) through the corresponding cluster. From the median value of 68 nm, we estimated the real average cluster size to be between 50 and 60 nm (15).

subsequent part from −2 to +8, shows fast recovery (Fig. 2E). These experiments suggest that SNARE motifs associating along almost their entire length are responsible for the reduced mobility of syntaxin, whereas its closed conformation and TMRs play no role. The similarity to the mechanism that directs syntaxin into clusters (7) indicates that reduced mobility is caused by the assembly of syntaxin into clusters.

As discussed above, FRAP does not differentiate whether recovery results from diffusion of entire clusters or from individual syntaxin molecules (or small oligomers) exchanging between immobile clusters. To address this question, we studied the dynamics of syntaxin 1A–GFP clusters. In this experiment, diffraction-limited spots, composed of a few individual clusters, were monitored that should reorganize, move, or show intensity fluctuations if clusters are mobile. To avoid membrane motions caused by cellular dynamics as, for example, actin cortex reorganization, we used native plasma membrane sheets in

which syntaxin mobility is indistinguishable compared to that of intact cells (fig. S4). Syntaxin spots did not change over minutes (Fig. 3), suggesting that fluorescence recovery occurs via exchange of syntaxin molecules between clusters. Together, these data show that free and clustered syntaxin molecules are in dynamic equilibrium with each other and all that is needed for clustering are weak homophilic interactions between plasmalemmal syntaxin molecules. Because strong overexpression of syntaxin increases cluster number rather than cluster size and does not generate a uniform syntaxin distribution (7), it is unlikely that other proteins are involved in the clustering mechanism. We therefore asked whether size and dynamics of such microdomains could be governed by simple physical principles rather than by elaborate layers of biological regulation. In the first scenario, clusters would form by self-organization solely depending on weak attractive forces involving homophilic SNARE motif interactions (likely

supported by cholesterol) that are balanced by repulsive forces that may include steric hindrance due to crowding.

To test whether this is possible, we simulated FRAP experiments by Brownian dynamics (Fig. 4, A and B) using a simple interaction potential between individual syntaxin molecules (Fig. 4B inset, bold line). An additional repulsive component was introduced, which strengthens with cluster size (Fig. 4B inset, dashed lines showing the resulting potentials). The known concentration of syntaxin [about 1800 molecules per μm^2; see also (15)] was used, and syntaxin diffusion was assumed to be similar to that of the construct lacking the cytoplasmic part, which had been shown previously not to participate in syntaxin clusters (7). Of the two adjustable parameters, the effective attraction and the strength of the repulsive component, only those parameter combinations were considered for which the simulations equilibrated at the experimental cluster density. For each of the allowed combinations, the sim-
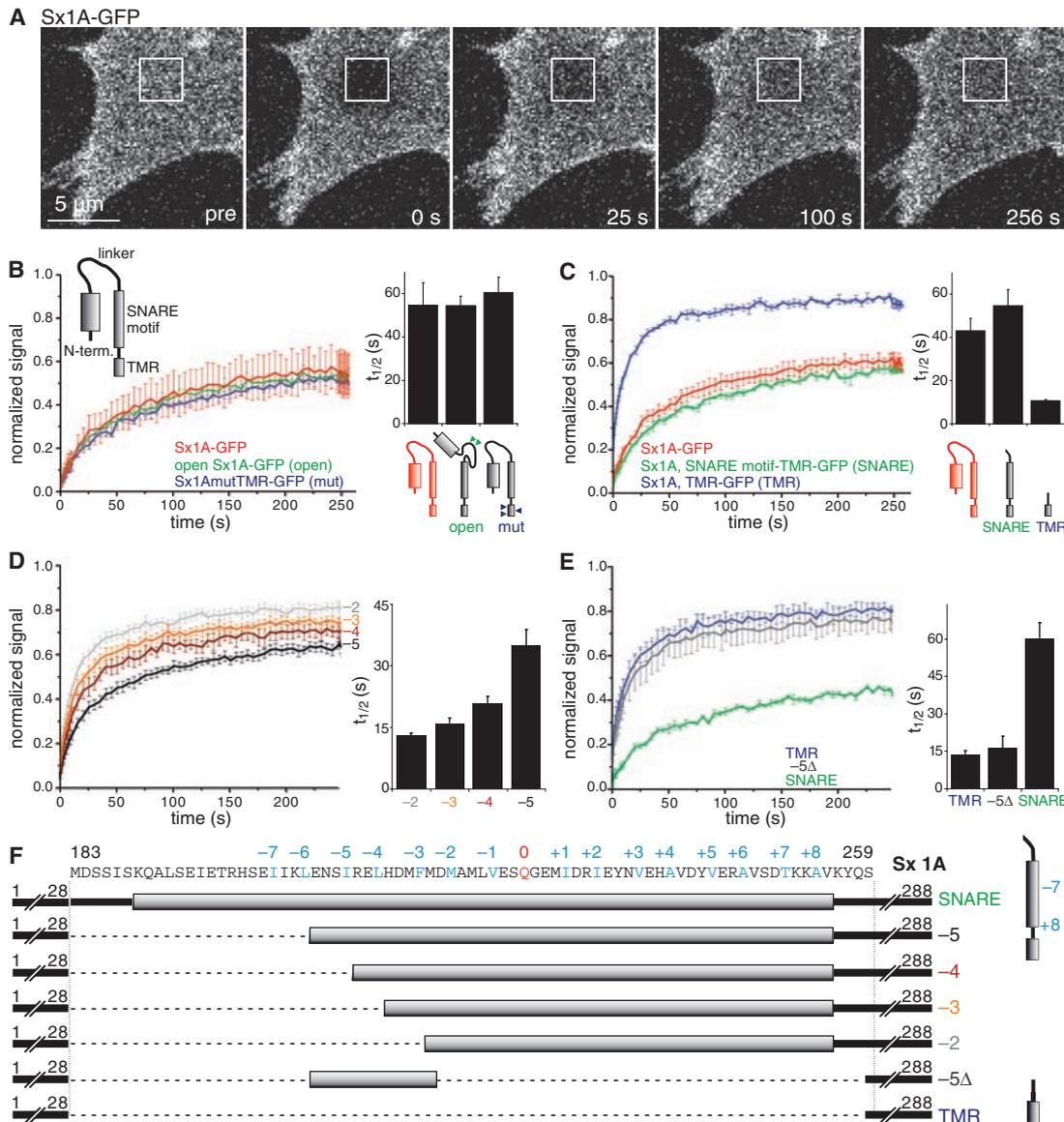
Fig. 2. Syntaxin 1 mobility is determined by the clustering reaction. (**A**) Confocal images from the basal plasma membrane of a PC12 cell expressing GFP-labeled syntaxin 1A. A squared region was bleached and FRAP was monitored. In one experiment, traces from individual cells (fig. S6) were averaged and fitted, and the recovery half time was determined. For each set of experiments [(B) to (E); n from 3 to 5 independent experiments), the means ± SEM of the recovery half times and the trace obtained by averaging the single experiments are shown. Syntaxin 1A (S × 1A) was compared to point mutants (**B**) or deletion derivates (**C**). (**D** and **E**) Testing the constructs indicated in (**F**), we studied the mechanism by which the SNARE motif controls mobility in further detail. Construct −4 is significantly different from −2, −3, and −5 ($P < 0.05$, paired t test, $n = 5$). (**F**) Numbers −7 to +8 refer to amino acids (24) (highlighted in blue and red) participating in layers of interaction in a hypothetical SNARE core complex (25).

ulation equilibrated at different amounts of syntaxin molecules per cluster and hence different fractions of free syntaxin, as indicated in Fig. 4B. With proper selection of the free syntaxin fraction, perfect agreement with the measured recovery curve was obtained (Fig. 4B, green curve). This shows that the observed self-organizing process can be explained in terms of simple interactions. Further, an average cluster size of 75 molecules is pre-

dicted by the simulation, with the remaining circa 300 molecules/μm^2 (corresponding to 16%) diffusing mostly individually between clusters. Exchange between clustered and freely diffusing molecules is governed by a distribution of dissociation time constants (fig. S5) with an average rate constant of $\langle k_{off} \rangle = 25,000/s$. Although only a small fraction of syntaxin is freely diffusing, a much higher degree of fluorescence recovery is reached be-

cause both pools of syntaxin are in equilibrium with each other. Moreover, clusters become immobile during the simulation within diffraction-limited resolution, another characteristic that is consistent with our experimental data.

Whereas the molecular basis for attractive forces can be readily explained by homophilic interactions of the SNARE motif, the origin of repulsive forces is less obvious. An in silico model of 75 open syntaxin molecules, oligomerized tightly via their SNARE motifs (Fig. 4C, left), offers a plausible and consistent explanation. In this model, the bulky N-termini would cause syntaxins to adopt a half-closed conformation at the rim of the cluster, resulting in a bunch-like structure. The 50-nm diameter of the structure formed by the N-termini, which contain the epitope for antibody staining, agrees with the cluster dimensions measured by STED microscopy. In this structure, molecules are conformationally constrained, and steric hindrance complicates attachment of more molecules with increasing cluster size. This effect would set an upper limit for the degree of oligomerization and provides a molecular explanation for the repulsive forces in the simulation. Further, it explains the immobile fraction of syntaxins in terms of slow release of inner molecules. Lastly, the bunchlike structure predicts that overexpression

Sx1A-GFP cluster dynamics on membrane sheets
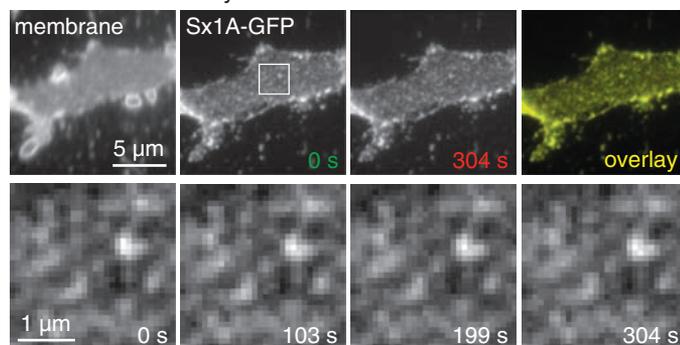
Fig. 3. Mobility of syntaxin clusters. Membrane sheet generated from a syntaxin 1A–GFP–expressing PC12 cell. A 5-min time-lapse experiment using epifluorescence microscopy was performed. Top left, 1-(4- trimethyl-ammoniumphenyl)-6-phenyl-1,3,5-hexatriene (TMA-DPH) staining for phospholipids of the membrane sheet. Middle and last images, first and last images of the GFP channel and corresponding overlay. The Pearson correlation coefficient of the first and last image was calculated, indicating high similarity [0.82 ± 0.11 (mean ± SD; $n = 16$ membrane sheets)]. Bottom images show magnified views of the boxed region (top) at indicated times.
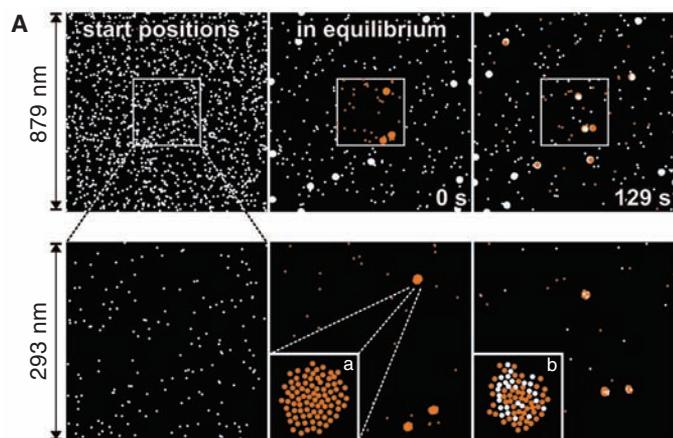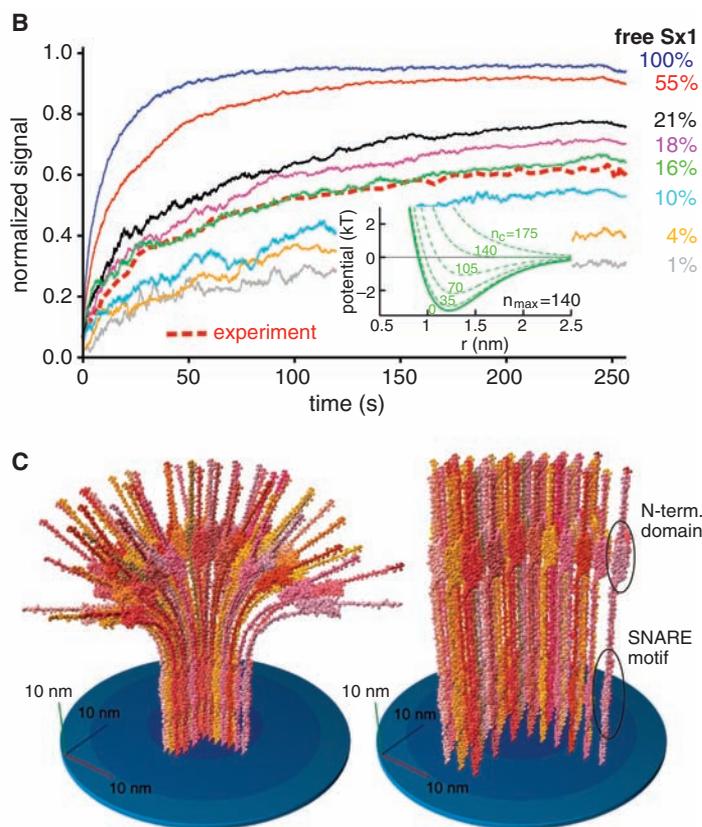

Fig. 4. Brownian dynamics simulation and in silico reconstruction of supramolecular syntaxin. (**A** and **B**) Simulation of lateral syntaxin diffusion by Brownian dynamics. Starting from a randomly chosen distribution [(A), left] and governed by an assumed interaction potential [(B), inset], spontaneous syntaxin clustering occurred and was followed in the simulation until thermodynamic equilibrium was reached [(A), middle]. Subsequently, fluorescence recovery [(A), right] after simulated bleaching (orange) of the central area [(A), middle] was monitored and averaged over several runs [(B), solid lines]. The effective syntaxin interaction strength and the strength of the repulsive component were varied until agreement with both the experimental cluster density and the measured recovery kinetics (dashed red line) was reached. Inset in (B) shows exemplary interaction potentials for various cluster sizes n_c at $n_{max} = 140$ (15). Attractive interactions occur at $n_c < n_{max}$. Insets in lower images of (A) (length of 14.7 nm) show the repopulation of a bleached cluster (inset a) with unbleached (white) syntaxins (inset b). Please note that at diffraction-limited resolution, images of the clusters appear blurred, resulting in spotty signals (Fig. 1A) with diameters of several hundred nanometers (about the size of the inset box). For this reason, in Fig. 3 cluster motions over small distances cannot be detected. (**C**) In silico reconstructions of supramolecular syntaxin.

of syntaxin increases the number of clusters rather than their size, which is in agreement with previous observations (7). In contrast, a hypothetical cylindrical syntaxin arrangement (Fig. 4C, right) would not explain our findings.

The self-organization model shows that a simple balance between weak homophilic interactions and a repulsive component can explain all available experimental data on the composition and the dynamics of syntaxin clusters.

Syntaxin clustering via self-assembly is likely a paradigm that applies to a variety of membrane protein clusters. Like the syntaxins, many other membrane proteins are known both to form clusters and to homo-oligomerize in vitro via their cytoplasmic domain. Examples include structurally diverse proteins such as synaptotagmins (13, 20) and receptors (4, 21) (containing single transmembrane domains), anion transporters [e.g., (22)] containing multiple transmembrane domains, and proteins such as reggie with lipid anchors [e.g., (23)]. The tendency to form homo-oligomers in solution would be enhanced in the plane of a membrane where membrane anchoring orients the molecules ideally for oligomerization. Hence, in the membrane self-association is enforced, leading finally to nanodomains containing many copies of the self-assembled membrane proteins. Thus, just as for the syntaxins, homo-oligomerization will likely lead to cluster formation for any membrane protein that can self-associate in solution.

The concept of clustering via self-assembly is not restricted to membrane proteins oligomerizing via their cytoplasmic domain. Rather, it can be widely applied to membrane proteins oligomerizing via their transmembrane or extracellular domains, with the only prerequisite being that in these cases there would be additional protein domains causing steric crowding or other repulsive forces, as, for example, accumulating charges.

As outlined above, the mechanisms underlying the high degree of membrane micropatterning are not well understood for most membrane proteins. With syntaxin 1 as an example, we present a conceptual framework for the description of protein domains in membranes. This biological principle is expected to explain a considerable part of the compositional variability of membrane protein clusters and hence will help to advance our understanding of membrane micropatterning.

References and Notes
1. S. J. Singer, G. L. Nicolson, *Science* **175**, 720 (1972).
2. K. Simons, E. Ikonen, *Nature* **387**, 569 (1997).
3. A. Kusumi et al., *Annu. Rev. Biophys. Biomol. Struct.* **34**, 351 (2005).
4. S. Uhles, T. Moede, B. Leibiger, P. O. Berggren, I. B. Leibiger, *J. Cell Biol.* **163**, 1327 (2003).
5. M. Kai et al., *J. Biochem. (Tokyo)* **140**, 677 (2006).
6. S. H. Low et al., *Mol. Biol. Cell* **17**, 977 (2006).
7. J. J. Sieber, K. I. Willig, R. Heintzmann, S. W. Hell, T. Lang, *Biophys. J.* **90**, 2843 (2006).
8. T. Lang et al., *EMBO J.* **20**, 2202 (2001).
9. M. Ohara-Imaizumi et al., *J. Biol. Chem.* **279**, 8403 (2004).
10. S. A. Predescu, D. N. Predescu, K. Shimizu, I. K. Klein, A. B. Malik, *J. Biol. Chem.* **280**, 37130 (2005).
11. J. C. Lerman, J. Robblee, R. Fairman, F. M. Hughson, *Biochemistry* **39**, 8470 (2000).
12. S. W. Hell, J. Wichmann, *Opt. Lett.* **19**, 780 (1994).
13. K. I. Willig, S. O. Rizzoli, V. Westphal, R. Jahn, S. W. Hell, *Nature* **440**, 935 (2006).
14. G. Donnert et al., *Proc. Natl. Acad. Sci. U.S.A.* **103**, 11440 (2006).
15. Materials and methods are available on *Science* Online.
16. A. K. Kenworthy et al., *J. Cell Biol.* **165**, 735 (2004).
17. A. T. Brunger, *Q. Rev. Biophys.* **38**, 1 (2005).
18. R. Laage, J. Rohde, B. Brosig, D. Langosch, *J. Biol. Chem.* **275**, 17481 (2000).
19. I. Dulubova et al., *EMBO J.* **18**, 4372 (1999).
20. M. Fukuda, E. Kanno, Y. Ogata, K. Mikoshiba, *J. Biol. Chem.* **276**, 40319 (2001).
21. K. Kanazawa, A. Kudo, *J. Bone Miner. Res.* **20**, 2053 (2005).
22. D. Navaratnam, J. P. Bai, H. Samaranayake, J. Santos-Sacchi, *Biophys. J.* **89**, 3345 (2005).
23. C. Neumann-Giesen et al., *Biochem. J.* **378**, 509 (2004).
24. Single-letter abbreviations for the amino acid residues are as follows: A, Ala; C, Cys; D, Asp; E, Glu; F, Phe; G, Gly; H, His; I, Ile; K, Lys; L, Leu; M, Met; N, Asn; P, Pro; Q, Gln; R, Arg; S, Ser; T, Thr; V, Val; W, Trp; and Y, Tyr.
25. R. B. Sutton, D. Fasshauer, R. Jahn, A. T. Brunger, *Nature* **395**, 347 (1998).
26. The authors thank R. Jahn and S. O. Rizzoli for helpful suggestions on the manuscript, V. Westphal and J. Keller for help with analysis software, K.-H. Drexhage for providing the dyes Atto532 and Atto647N, and F. E. Zilly and M. G. Holt for gifts of a plasmid and a recombinant protein, respectively. T.L. was supported by a grant from the Deutsche Forschungsgemeinschaft (LA1272/2). S.W.H. consults for Leica Microsystems CMS, Gmbh, Mannheim, Germany.

Domain Architecture of Pyruvate Carboxylase, a Biotin-Dependent Multifunctional Enzyme

Martin St. Maurice,[1] Laurie Reinhardt,[1] Kathy H. Surinya,[2] Paul V. Attwood,[3] John C. Wallace,[2] W. Wallace Cleland,[1] Ivan Rayment[1]*

Biotin-dependent multifunctional enzymes carry out metabolically important carboxyl group transfer reactions and are potential targets for the treatment of obesity and type 2 diabetes. These enzymes use a tethered biotin cofactor to carry an activated carboxyl group between distantly spaced active sites. The mechanism of this transfer has remained poorly understood. Here we report the complete structure of pyruvate carboxylase at 2.0 angstroms resolution, which shows its domain arrangement. The structure, when combined with mutagenic analysis, shows that intermediate transfer occurs between active sites on separate polypeptide chains. In addition, domain rearrangements associated with activator binding decrease the distance between active-site pairs, providing a mechanism for allosteric activation. This description provides insight into the function of biotin-dependent enzymes and presents a new paradigm for multifunctional enzyme catalysis.

I n biochemical pathways, metabolites must be efficiently transferred between enzymes to avoid the energetic penalty associated with their loss to diffusion, degradation, or competing side-reactions. Particularly efficient transfer is afforded by multifunctional enzymes that directly transfer products from one reactive site to the next through tunnels and channels (1) or through the use of covalently attached prosthetic groups (2). Although the reactions catalyzed at the individual active sites of many multifunctional enzymes are well understood, few studies have detailed their complete domain architecture. Consequently, descriptions of intermediate transfer between active sites in multifunctional enzymes remain largely incomplete.

The multifunctional enzymes of the biotin-dependent family use a covalently attached biotin prosthetic group to directly transfer an activated CO_2^- intermediate between distinct active sites in several essential metabolic reactions (3). Some members of this enzyme family, including acetyl–coenzyme A carboxylase (ACC) and pyruvate carboxylase (PC), have recently attracted interest as potential targets in the treatment of obesity and type 2 diabetes (4, 5). Although several individual domain structures have been determined for various family members (6–9), the relative arrangement of these domains in a complete multifunctional enzyme remains unknown. PC is typically composed of three distinct functional domains arranged on a single 120- to 130-kD polypeptide chain. The three domains are an N-terminal biotin carboxylase (BC) domain, a central carboxyltransferase (CT)

[1]Department of Biochemistry, University of Wisconsin, Madison, WI 53706, USA. [2]School of Molecular and Biomedical Science, University of Adelaide, SA 5005, Australia. [3]School of Biomedical, Biomolecular, and Chemical Sciences, University of Western Australia, Crawley, WA 6009, Australia.

*To whom correspondence should be addressed. E-mail: Ivan_Rayment@biochem.wisc.edu